Self-Assembling Space Structures: buckminsterfullerene sensor nodes

Ariel Ekblaw* and Joseph Paradiso†
MIT Media Lab, Cambridge, MA, 02141

Self-assembly protocols hold great promise for aerospace structure development, offering a reduction in complexity, removal of manual construction steps and an increased flexibility for dynamic space-allocation and adaptive reconfigurations of the architectural base units. We propose a buckminsterfullerene self-assembling structure for deployment in zero gravity. This paper details our concept design, the sensor node and electronics design, the communication architecture, and preliminary parabolic flight tests on a proof-of-concept hardware prototype. This research advances towards a technology demonstration mission.

I. Introduction

THE future of human habitation in microgravity, from low Earth orbit (LEO) to the Asteroid Belt, lies in self-assembling, adaptive, additive and inflatable structures. Rather than transporting the weight of gantries and mechanical assembly cranes, we can lower payload weight, reduce assembly complexity, and revolutionize space-structure modularity by relying on these new modes of construction. In particular, the mechanism of self-assembly (for energy "favorable" state configurations) offers two critical benefits: first, a significant reduction to assembly risk and mission resource consumption, as construction of the structure does not require manual efforts via astronaut extravehicular activities (EVAs); second, if designed with reversibility in mind, the ability to dynamically detach and reconfigure into other shapes, providing a newfound, adaptive flexibility in the creation of space structures. Structures need not be "purpose-built," single use modules, but should instead feature extensible units that support reconfigurable architectures—we see this philosophy emerging more and more in the aerospace industry, from reusable rockets [1] to modular space structure design [2]. Self-assembling architectures will be based on fundamental assembly units, or tiles, that provide enough degrees of freedom for multiple structural arrangements while retaining the required specificity to generate a predictable suite of desired shapes. In the design of such a self-assembling system, we consider four key parameters: the base-unit tiles, the jointing method, the assembly protocol, and the holistic function of the structure.

For predictability of the assembly, the tiles must be standardized to certain sizes and polygon geometries that assemble to create desired macro-shapes. This calls for tiles in the form of "regular" (equiangular and equilateral) geometric building blocks, such as triangles or other simple polygons. The needs of a particular structure will determine the resolution of the assembly—a mesh of many small tiles for an approximation of a smoother surface, or a polyhedral composed of only a few, larger tiles for a coarser shape. In concert with this notion of pre-fabbed modularity lies an opportunity for optimizing the functional properties of different tiles for the aerospace structures context. Certain tiles can serve as sensor nodes, while others are augmented with imaging capabilities built in for remote-sensing or life-support system monitoring. While aerospace deployments will likely require heavy customization inside the structures (to meet the needs of occupants, storage, power generation, etc.), the exoskeleton of a self-assembling structure should rely on a standard suite of tiles with augmented functionality.

Beyond the properties and functional purpose of any individual base-unit tile, we must design a way for tiles to securely and reliably mate with neighbor tiles. This definition of jointing could take many forms, from magnetic joints that rely on aligned polarities and proximity for the magnetic forces to draw pieces together, to unique lock-and-key joints where compatible pairs snap in place, to interleaved edges where tabs slide into slots, to specially activated adhesives that bond matching tiles edges (or some combination of these and other methods).

Intimately related to the jointing mechanism is the self-assembly protocol. Options include: passive self-assembly, where tiles float around each other and assembly in a stochastic process; a tile-dispenser releases one tile at a time for a predictable feed of parts that accrue to a growing structure; a robotic-mediated control algorithm directs tiles toward each other at the optimum time and place; et cetera. These self-assembly protocols must be matched with jointing methods that correspond to the anticipated amount of time tiles would need to spend near each other, how much kinetic

*Graduate Research Assistant, Responsive Environments, MIT Media Lab
†Alexander W. Dreyfoos (1954) Professor of Media Arts and Sciences, Responsive Environments, MIT Media Lab, AIAA Senior Member

disturbance the system requires to circulate tiles past each other in assembly-favorable positions, the desired level of automation, et cetera. Appropriate pairs of assembly protocols and joint fittings (i.e. magnetic joints and stochastic tile dynamics, or lock-and-key joints with robotic-mediated assembly) will yield varying efficiencies—from the time it takes for the full structure to assemble, to the likelihood of incorrect bonding into local-minima structures.

Finally, the holistic function or end purpose of the assembled structure also drives key elements of the design. Will the resulting capsule need to be airtight to support human inhabitants (in which case the assembly jointing must be supplemented with additional sealing, or an inner pressurized layer)? Will the self-assembled structure serve as a docking bay for larger, more customized modules and thus require special interface tiles? If some of the tiles are bulkier than others to accommodate this docking, how does the variance in mass distribution affect the dynamics of the assembly process? The requirements for the holistic function therefore shape design decisions for the individual tiles, jointing method and assembly protocol.

This technology demonstration mission explores these four parameters for a self-assembling system and proposes a multi-year research effort to engineer and deploy test structures. We scale the research down to lab-bench size initially, with the intent to extrapolate the research to habitation structure scale. The first prototype, recently deployed on a November 2017 parabolic flight and scheduled for sub-orbital, enclosed launch in 2018, is a tessellated Buckminsterfullerene structure (or "buckyball") [3] that self-assembles stochastically in zero gravity via magnetic joints. Thirty-two polygonal tiles, augmented with sensor nodes, are released to swirl around each other in a contained volume and passively snap together, without the need for propulsion, guidance and navigation control, or advanced robotics. Placing this self-assembling structure in an aerospace mission concept, we design our Tessellated Electromagnetic Space Structures for the Exploration of Reconfigurable, Adaptive Environments (TESSERAE) to function as multi-use, low-cost orbiting modules. See Fig. 1 for a diagram of the TESSERAE deployment approach. With future stages of this project, we hope to build towards a critical space infrastructure for the next generation of zero gravity LEO habitats, asteroid mining support modules, staging bases for Martian on-surface exploration and more.

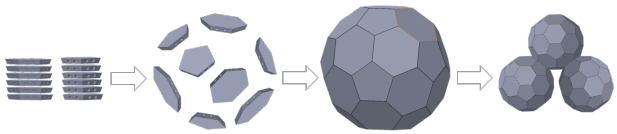

Fig. 1 TESSERAE deployment protocol: Ship flat –> free floating tiles –> TESSERAE assembly –> constellation

II. Background

This research builds on prior work in several fields, including materials science, mechanical engineering, architecture and design, bio-inspired robotics and emerging fabrication tools in the Aerospace industry. Neil Gershenfeld's lab in the MIT Center for Bits and Atoms (CBA) has demonstrated innovative assembly protocols for lattice structures, from modular 3D circuits [4] to "sparse, space-filling" wireframes [5]. Though the assembly for the 3D circuits is still done programmatically via a machine, rather than self-assembled, our research approach can learn from the jointing methods that connect various planes of the circuit together. Langford and Ghassaei, of the CBA, demonstrate a pattern of interlocking tabs for these circuits that could be extrapolated to other assembly protocols. Furthermore, their focus on standardized, modular units with pre-set functions defines an approach that we will also pursue, particularly for the tile base units that comprise the buckyball assembly. The Gershenfeld lab has also demonstrated reversibility protocols for lattice structures, notably carbon-fiber reinforced units that feature reversible shear clip joints [6]. We consider a similar principle, relying instead on magnets to provide joint connection and subsequent "reversibility" or detachment flexibility.

The MIT Self-Assembly Lab explores self-assembly in a bio-inspired context, with plastic "chiral assemblies" that are shaken stochastically into final form to simulate biomolecular processes [7]. In collaboration with Autodesk, this work shows potential for embedding logic in many small parts, that when brought into contact with sufficient randomness and circulation, can dynamically self-assemble into predicted shapes. In a different approach, their work on self-folding surfaces uses built-in restoring forces and spring forces to actuate a final shape after an initial perturbation [8]. Both methods, stochastic assembly and force-loaded joints, show great promise for our work that takes these previously demonstrated mechanisms into the zero-gravity realm. Without the need to counteract the force of gravity, we anticipate that similarly modeled base units (in our case, polygon tiles with magnet joints) will assemble in much

shorter time-scales.

In addition to motion-driven or stochastic self-assembly, the Self-Assembly lab explores fundamental units where the final-state configuration logic is embedded in the fabrication of the constituent parts. In "Biased Chains," a connected chain of plastic nodes can be held at the end and shaken into a desired sequence of folds [9]. Though the individual nodes are still connected manually by hand, subsequent configuration states of the chain are encoded via the "biased direction" introduced in each base unit. We take a similar approach in our work and push this further by removing manual construction steps. By carefully designing the tile geometry (size, dihedral bonding-edge bevel) and the magnet polarity jointing, we embed logic in the assembly protocol and can constrain the assembly to a buckminsterfullerene configuration.

Tiles in our system are augmented with custom sensor PCBs (Printed Circuit Boards). Our early circuit designs draw on environmental sensing nodes from the Paradiso Lab, deployed in nature and optimized for low power consumption [10]. We note prior art to build on in scalable communication and data architectures for swarm dynamics, coming out of Radhika Nagpal's Self-Organizing Systems Research Group at Harvard, and their work on "Kilobots"—a bio-inspired robotic swarm [11]. Their work explores self-assembly in a different context, with a focus not on mechanical assembly but rather the data architecture, algorithmic development and start-up tasks (i.e., power charging) required for a swarm of over a thousand small robots to perform tasks and communicate as a collective. The Kilobots are currently restricted to a 2D plane, but offer an enlightening example of how to scale communication and power-management tasks across many nodes. We anticipate an interest in swarms of self-assembling tiles in 3D space and a progression from stochastic-mediated assembly to a robotic-mediated protocol in the future. Recent work in IR-mediated interactivity between modular, PCB-augmented tiles also informs our sensor node design [12]. Though we ultimately settled on Bluetooth Low Energy and a different communication architecture, we note the IR emitters approach as an additional functionality to consider for future work. We also note a legacy in scalable distributed sensor nets built into modular structures or made into sensate "skins" coming out of the Paradiso Lab [13].

In the aerospace structures context, we will likely rely on pre-existing inflatable container concepts (for containment of the tiles while assembling), such as the Bigelow Expandable Activity Module [14]. We also note related work in origami and unfolding structures [15], and are open to exploring this design paradigm as a complement to the self-assembling primary structure. While our mechanism of self-assembly is distinctly different from recent tensegrity-based approaches, we note extensive prior art in the area [16], [17]. While our TESSERAE approach should prove more straightforward to deploy (less cables, simpler mechanical system, energy-favorable modular self-assembly rather than fixed, tensioned parts), we are open to integrating with future tensegrity structures and will consider interoperability with these proposals in our habitat design. Recent developments out of Silicon Valley startup Made in Space lead us to envision a future where our self-assembling tiles are even fabricated in-situ, via advances in zero gravity 3D printing and in-orbit material recycling [18].

III. System Design

At this stage of concept development, we identify three primary areas of focus: self-assembly as a building mechanism in a multi-part, stochastic system; sensor node design to augment the structure ("smart assembly"); and a communication architecture design to enable multi-node sensor exchange and uplink/downlink. This paper will review our approach in each area, treating each as a subsystem to optimize in a future zero gravity-deployed aerospace structure.

A. Self-Assembly

The initial phases of prototype deployment focus on the "buckyball" structure as the target assembly shape. The buckyball structure recalls the architectural geodesic dome, a shape that describes both an energy-favorable configuration state in nature and a visual form that has intrigued imaginations for decades, from biospheres to concert halls. Buckyballs, as sphere approximations, offer highly efficient space-filling options (a critical consideration for orbiting deployments). This shape can be assembled from 12 pentagonal and 20 hexagonal tiles, with certain key tile features that help to constrain the geometry and ensure a successful assembly.

The mechanism of self-assembly relies on magnetic jointing between the tiles, each 3D printed to a strict tolerance with recessed holes for the 3mm neodymium cubes. Tiles measure 5-6cm across, depending on the hexagonal or pentagonal geometry. Each tile edge is beveled at the proper dihedral angle to establish the expected buckyball curvature, as tiles begin to bond together. This beveling also establishes a flush mating surface and exposes two recessed magnets on each mating edge that draw tiles together for bonding. See Fig. 2 for an example of the individual tile part and overall geometry.

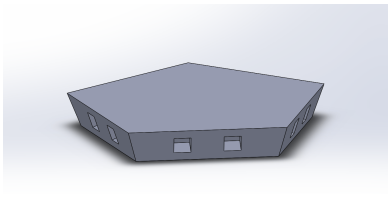

(a) Pentagon SolidWorks model

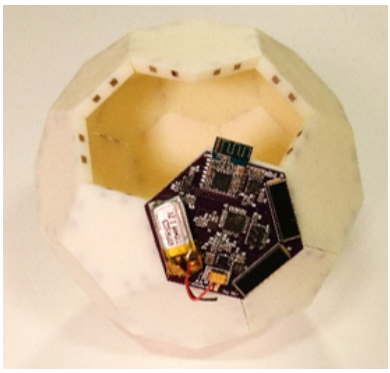

(b) Prototype assembly at 13cm diameter

Fig. 2 Self-assembly individual tile and aggregate example

The spatial configuration of north and south polarity for these paired magnets defines a system of mating joints, guiding the proper neighbor tiles towards each other and ensuring that incorrect tile matches do not bind (e.g. matches that might lead to a partial, incorrect or clumping shape rather than the full assembly). Key to the modularity of the structure is the tunable nature of the magnet-magnet bonding: while initial prototypes rely on passive magnets, we design the future iterations to have electromagnetic jointing to facilitate reconfigurable shapes. Turning magnets on or off in a controlled fashion will allow us to detach certain tiles, or reattach others, as needed for mission operations.

Our design for the spatial magnet arrangements makes use of the north-south polarity to define the minimum number of distinct joints that will force a C60 buckyball structure. This approach relies on the simplicity of magnetic jointing and geometric structure symmetry, thus avoiding complication (at least for initial prototypes) with robotic-mediated controls. This focus on joint-logic simplicity—finding the "minimum number of distinct joints" to constrain the geometry—is critical for optimizing the assembly probabilities in a stochastic system. Rather than every joint being unique, any two hexagons can bind together on certain faces and any hexagon can bind to a pentagon on the other faces.

The tiles are designed to be released into a temporary, inflatable container and allowed to float free. The constituent parts then passively, stochastically self-assemble without manual or robotic-mediated guidance. It is this simplicity of construction that offers the TESSERAE a significant reduction in resource consumption, leading us to explore this approach further as an inherently scalable in-orbit architecture (compared with prior models such as the bespoke, custom module-based International Space Station).

B. Sensor Node Design

The tiles that comprise the assembly offer a natural surface for distributed sensing technology, both in the current prototype and for subsequent scaled-up deployments. The prototype structure benefits from feedback on its assembly status (inertial measurements tracking tile motion, Time of Flight ranging determining whether the structure has closed successfully, etc.), and can also serve as a remote sensing platform. Bluetooth Low Energy (BLE) communication between the prototype sensor nodes will enable an emergent sensor-network functionality when all tiles have properly assembled. In subsequent versions, these tile-embedded sensor nodes could be used to support secondary applications post-assembly, such as radiation detection, life support system monitoring and on-demand, adaptive changes to the structure via coordinated control of the electromagnets.

Each prototype tile is augmented with a robust, independent sensor node, designed to communicate with other tiles and a base station. Selection of desired sensing elements include IMUs (Inertial Measurement Units), Hall sensors, LIDAR Time-of-Flight sensors and a microphone (for capturing interior sounds post-assembly), with a subset of these sensors currently implemented on the prototype circuit boards discussed below. Small form factor CMOS, CCD and spectroscopy chips are in evaluation for special-use tiles. While we primarily select components from well-established sources, we are also closely watching emerging research in nanomaterials, fibers and battery technology. We believe these developments, notably experiments in the Fink fiber lab [19] [20], hold promise for the extreme operating regimes of zero gravity and in-vacuum operation. Functional fibers (with sensing, energy storage or communication capabilities), printed circuitry and flexible electronics could augment traditional circuit design in our assembling tiles context.

Following these identified sensing needs, a subset of components was carefully selected, taking into account several metrics that flow from our payload requirements and prototyping feasibility: functionality and contribution to the sensing application, power consumption, package size, and cost. With the latest revisions of our custom PCB, we hoped to keep costs low and fit all components into the fixed dimensions of the base hexagon tile. This allows us to mount the PCBs onto the hexagon tiles as affixed sensor nodes that can track the lifecycle of the assembly—from initial tile release, to full structure configuration, to steady-state sensor reporting. Keeping costs low allows us to develop a proof of concept plan for hundreds or thousands of these nodes, creating a swarm of tiles from which structures can stochastically arise. Keeping power consumption at a minimum is also critical for this project, as we envision deploying the sensor node tiles with small, onboard batteries and running for multi-hour durations for data collection and reporting. Our approach employs an energy harvester solar power charging chip, paired with solar cells on the external tile surface, to test recharging via incident sunlight during subsets of a future orbit. See Fig. 3 for a summary of component selection. Sensor and chip information in the below chart is gathered from the following datasheets (ATMEGA 328p [21], LSM303dlhc [22], L3G4200dtr [23], HM-11 BLE [24], BQ25570 [25], battery [26], KXOB22-01X8F [27]). Future additions to the circuit will include the microphone and LIDAR sensors (discussed in more detail below).

The simplified schematic flow diagram shown in Fig. 4 summarizes the main power rail, I2C connections for the sensors, SPI connections for the programming pins and UART Rx/Tx communication for the BLE module. The battery and PV cells feed into the BQ25570 and are regulated down to supply a consistent 2.8V to the board (power and logic).

Key Components	Purpose	Notes on selection
AT Mega 328P	IC	Chosen for sufficient pin number, low power modes and familiarity/ease of prototyping
LSM303dlhc	6 DoF Accelerometer + Magnetometer	Includes a low-resolution temperature sensor, 16 bit
L3G4200DTR	Gyro	Low power, 3 axis angular rate sensor, 16 bit
HM-11 BLE	Bluetooth Low Energy module	Convenient prototyping model, good documentation of AT commands
BQ25570	Energy Harvester/Solar Charging chip	Chosen for notable low power consumption, to avoid constant drain on the battery (under 5nA)
3.7V Li-ion, 105mAh	Battery for onboard power	Chosen primarily for small footprint, 11.5mm x 31mm and matching mAh for desired duration of battery-powered operation.
KXOB22-01X8F	PV cells	Chosen primarily for small footprint, 22mmx7mm, and for matching open circuit voltage (4.7V) to that of the BQ25570

Fig. 3 Component selection chart

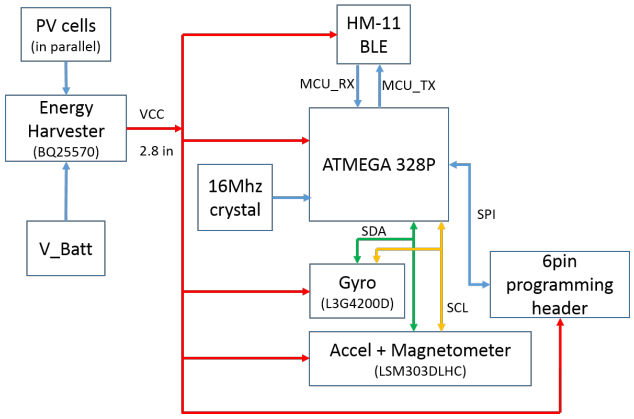

Fig. 4 Circuit flow diagram

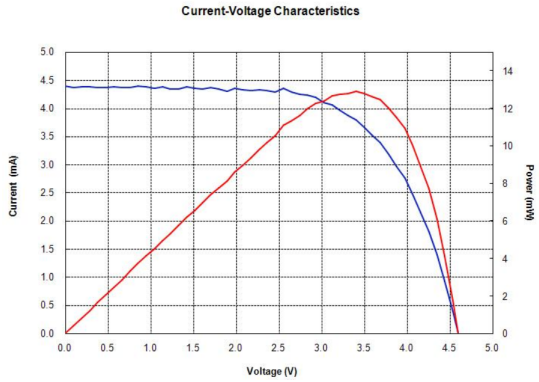

(a) IV Curve for KXOB22-01X8F photovoltaic cell [27]

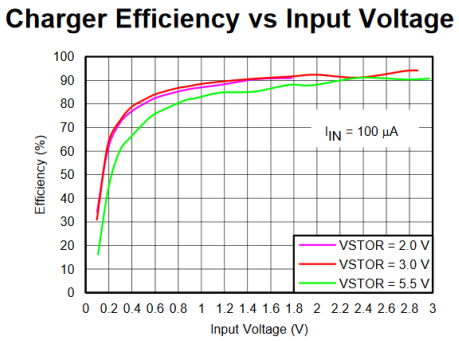

(b) Charger efficiency plot for the bq25570 [25]

Fig. 5 Solar charging performance analysis.

Table 1 Current draw by operating mode

Component	Full (mA)	Sleep (uA)
ATMEGA 328p	0.2	0.75
HM-11 BLE	15	600
BQ25570	negl.	.445
LSM303dlhc	0.11	1
L3G4200DTR	6.1	5
TOTAL	21.4	607

1. Minimizing Power Consumption

A key consideration for this board design was to keep the power consumption as low as possible, in order to achieve maximum operating duration with a relatively small li-ion battery. In a significant redesign over our initial proof-of-concept board, this v2 design incorporates two monocrystalline photovoltaic cells (in parallel), selected to match the max open-circuit voltage of the MPPT bq25570 and provide supplementary re-charging for the battery. The photovoltaic cells (PVs) are selected to provide more than the desired power output, to account for losses due to the imperfect efficiency (22% solar cell efficiency for the KXOB22-01X8F). The KXOB22-01X8F is also notable for its wide spectral sensitivity (300nm-1100nm), therefore providing functionality in both indoor and outdoor settings [27]. While initial deployment of this prototype will be confined to indoor settings, we may explore this same PV cell for use in time-limited, early external deployments (should this model evidence robustness for in-vacuum deployment).

The BQ25570 is notable for its impressively low "full operating quiescent current" state (488nA) and its approach for dynamically managing the load to meet the max power "sweet spot" on the PV cells' IV curve (Fig. 5a). As noted in the datasheet, the BQ25570 device is "specifically designed to efficiently extract microwatts (uW) to milliwatts (mW) of power generated from a variety of high output impedance DC sources like photovoltaic solar or thermal electric generators (TEG) without collapsing those sources" [25]. In addition, we have designed the circuit to try and achieve the max charging efficiency regime for a given value of VSTOR (Fig. 5b). Texas Instruments provides guidelines for choosing the resistors that populate the key VBAT_OV (max storage element voltage), VBAT_OK_HYST (threshold voltages for normal operation), and VOUT (the input VCC for the downstream circuit) lines, depending on the nominal battery voltage and desired output voltage [28]. These values also affect the lifecycle of the battery (number of charging cycles, discharging rate, etc.) and our goal is to optimize for battery longevity (as the tiles will be remote-deployed with no means to replace the power supply). We regulated the VCC down to 2.8V, to match the optimal operating regimes for the sensors and AT Mega 328p, per their datasheets.

The low total current draw for this board (see Table 1) lies well within our goal range, defining an achievable load for our chosen li-ion battery. At peak current draw, we could run for just under 5 hours with the 105mAh capacity of the

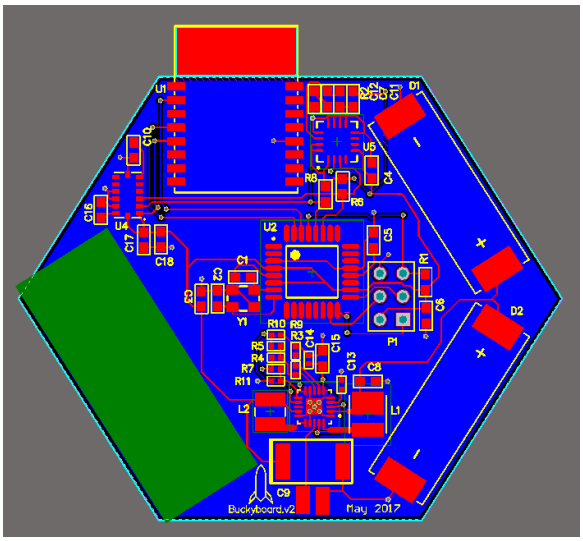

(a) PCB layout in Altium

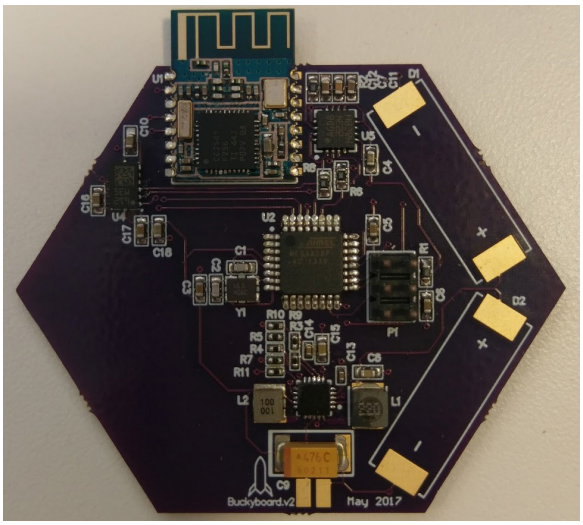

(b) Populated board, with space reserved for solar panels and small battery

Fig. 6 Sensor node PCB circuit design

chosen batteries. The addition of the KXOB22-01X8F PV cells provides a modest amount of supplementary current: 3.8mA each, at peak performance. Together, the PV cells could supply a maximum of 36% of the current draw, in the current configuration.

This power source and power consumption model gives more than ample operating time for the expected assembly period, and a subsequent period of low-power and sleep-mode operation. We note that the power in both modes (full and sleep) is dominated by the HM-11 module. For subsequent revisions, we may seek out a lower power version, or power it directly off a pin from the micro-controller to be able to power it off completely when not in active use.

2. Time-of-Flight Sensor Selection

In addition to the Inertial Measurement Unit (IMU) sensor packages, we are interested in rangefinding between tiles as they dynamically assemble. We are also interested in measuring the distance between tiles once they are stationary, to confirm that the anticipated buckyball configuration, with proper steady-state separation between tiles, has been achieved. These requirements led us to consider various Time-of-Flight (ToF) sensors, which use a LIDAR approach. We anticipate placing a ToF sensor on the underside surface of each tile (the surface that faces the interior of the structure) and we will de-conflict crossing pulses via a time-shifting regimen in the programming code.

While we ultimately selected the VL6180x [29] and VL53L0x [30] ("sister" chips, varying primarily in their range of detection) for testing, we also considered other gesture, ambient light and IR ranging sensors (APDS-9960 RGB gesture sensor, VCNL 4000) before settling on ToF sensors for their improved precision and applicability for our use case. The two sensors are both notable for their small size (a benefit to our spatially-constrained PCB design) and their ability to report ranging data independent of target reflectance. Both modules are also designed for low power operation.

Our ToF sensor testing analyzed the differences in full scale range, accuracy and precision between the VL6180x and Vl53L0x. We were motivated to complete this analysis due to the widely varying reports on each sensor's actual performance (e.g. for the VL6180x, Adafruit quotes a 5mm-20cm range [31], Sparkfun quotes simply a "25 cm total ranging area" [32] and the ST datasheet for the chip quotes 0-10cm for standard operation [29]). We ultimately chose the VL6180x based on our experimental results. This sensor operates well in the range we are most interested in (0-20 cm), and though we observed a notable fixed offset, this is easily corrected for via a simple shifting calibration. The average standard deviation across three separate ranges (with multiple repeated measurements at 0cm, 5cm and 10cm) was lower than that of the VL53L0x. In addition, we value the lux sensor built into this chip, in contrast to the VL53L0x which had no additional ambient light detection and reporting capability.

3. Sensor Node Integration with Assembly Tiles

The custom PCB sensor nodes are currently manually bonded to the outer surface of the 3D printed tiles, when necessary for testing or deployment opportunities. See Fig. 6 for the current PCB layout and a close-up of a populated board. This circuit design is in a transition stage; some features (such as overall power budget) are designed with a LEO satellite orbit in mind, and other features (such as initial component selection) are not yet vacuum-proofed, nor orbital-temperature resilient. This is because we are anticipating internal deployment testing inside the ISS before progressing to external orbital deployment, and this board will continue to evolve through our spiral process for prototype development.

As we explore material selection for the tiles, our goal is to find ways to natively embed a suite of sensors into the manufacturing of the tiles themselves–rather than adding the sensor nodes as separate, external components. By integrating sensing with the material, we can improve the modular properties of the structure and build a useful level of redundancy and robustness into our designs.

C. Communication Architecture

A proof of concept, miniaturized PCB has been developed to test the above sensor node design with a BLE (Bluetooth Low Energy) network topology for sensor-sensor and sensor-to-central downlink node communication. After careful consideration of the various wireless radio modes often considered in similar project contexts (xBee, ZigBee, WiFi, etc.) we have chosen BLE 4.0 for its extremely low power operating states, the adaptive frequency hopping (AFH) capability to avoid data transmit channel collisions, and its relative ubiquity in consumer devices [33]. Early deployments of our prototype will likely be tested in environments where other BLE devices are present (an onboard computer for sub-orbital testing, astronaut laptops, etc.) and we will greatly benefit from the ease of connecting with and interfacing with proximate devices for data transfer. In addition, the bandwidth limits, range and network size all fit our requirements. We do not require the thousand-node support that Zigbee offers, at this time. While we have initially designed the communication architecture in a standard BLE star topology (a central node communicating and dynamically pairing with multiple peripheral nodes), we look forward to exploring the mesh-supported topologies in BLE 5.0. Please see Fig. 7 for a comparison of the available communication modes.

Name	Bluetooth Classic	Bluetooth 4.0 Low Energy (BLE)	ZigBee	WiFi
IEEE Standard	802.15.1	802.15.1	802.15.4	802.11 (a, b, g, n)
Frequency (GHz)	2.4	2.4	0.868, 0.915, 2.4	2.4 and 5
Maximum raw bit rate (Mbps)	1-3	1	0.250	11 (b), 54 (g), 600 (n)
Typical data throughput (Mbps)	0.7-2.1	0.27	0.2	7 (b), 25 (g), 150 (n)
Maximum (Outdoor) Range (Meters)	10 (class 2), 100 (class 1)	50	10-100	100-250
Relative Power Consumption	Medium	Very low	Very low	High
Example Battery Life	Days	Months to years	Months to years	Hours
Network Size	7	Undefined	64,000+	255

Fig. 7 Communication protocol comparison chart [34]

BLE transmits and receives in the 2.4Ghz band, with 37 data connection channels and three "advertising" channels [33]. While the stated max bandwidth is 1Mbit/s, we expect an actual operating max of .27Mbit/s, and as discussed below, our data transfer rates will be well below this bandwidth cap.

In our BLE architecture design, we consider five primary areas: the sensor data packet; packet transmission timing and data flow rate; network topology; power optimizations; and redundancy and backup transmission contingencies.

1. Sensor data packet

To design the data packet, we first determine what data we wish to transmit from the sensors. At minimum, each tile node includes an accelerometer, magnetometer and gryo (16 bits each, across three axes each), for a total of 18 bytes of sensor data. We anticipate using another 4 bytes for ID event tracking and error variables, bringing us up to 22 bytes total. The data packet will be transmitted with parameter coding (numbers preceding each transmitted value, to establish a legend for the data transmission), allowing us to filter on certain parameters and flexibly handle partial

packets if some data is missing in any given transmission.

2. Packet transmission timing and data flow rate

We anticipate two separate regimes for data communication, one during active assembly and one during steady-state, post-assembly. For the former, we intend for each sensor node's BLE module to send IMU sensor information no slower than every 500ms (our data loggers report data at a much higher frequency, and we will consider more frequent data communication between tiles as justified). Thus, any individual tile is sending a mere 352 bits/second. For an aggregating central node, in the most condensed central-peripheral configuration (discussed in more detail below) this yields a max data receiving rate of:

44 bytes/sec x 31 peripheral tiles x 8 bits/byte = 10.9 kbits/s

This transmission rate is well below the BLE bandwidth limit noted above, and should not push power consumption for the BLE module outside of expected ranges. For the steady-state mode, the nodes will report IMU data once a minute, allowing us to put the boards into an extremely low power state between transmissions. Because we plan to gather all the data from sensors for post-processing and do not require live data reporting for actuation of other parts of the system (the assembly is all passive), we do not envision any power consumption or delays from on-chip data processing.

3. Network topology

This aspect of the BLE communication architecture design defines how many nodes are "central," how many nodes are "peripheral," and how these nodes are connected in pairwise relationships. The most condensed topology we consider would be a single central node and 31 peripheral nodes (for a total of 32 tiles) in a star configuration. The BLE spec supports this many concurrent connections, but the primary limiting factor would be identifying a chip that supports such a topology. An alternative arrangement explores naming additional central nodes, and distributing peripherals around these. For example:

12 pentagon tiles: 2 centrals, 10 peripherals (5 peripherals per central)

20 hexagon tiles: 4 centrals, 16 peripherals (4 peripherals per central)

As discussed in the following section, this second topology may aid in de-conflicting transmission channels, and white-listing certain peripherals for connection to their matching central node.

4. Power optimizations

To avoid having to establish a full data transfer connection between each central and peripheral tile node (which requires the full power profile for the BLE module), we can instead rely on BLE's advertising mode. This allows peripheral sensors to advertise up to 37 bytes of data to any centrals in their area (actually only 31 bytes, after BLE overhead) [35]. See Fig. 8 for a breakdown of the advertising data packet. Because we need only advertise 22 bytes of sensor and context data at any one time, this advertising packet fits our minimum data communication needs. We may subsequently include additional sensor data in the node-node communication channels. Notably, BLE modules in advertising mode consume significantly less power. This is an emerging BLE communication approach, perhaps best known from Apple's ibeacons, which rely on advertising packets to push data to passerby BLE receivers [36]. Fortunately, the BLE spec also includes a way for central nodes to indicate acknowledgment of advertising data from peripheral nodes, which we will use for redundancy designs in the following section. When not actively pushing advertising data, nodes will return to a standby state from which they can re-enter advertising mode or receive a request for full connection to a central node, depending on our needs for data transfer. Figure 9 shows how BLE nodes can shift between these various power and communication states.

5. Redundancy and backup transmission contingencies

In order to ensure robust data communication channels, we would like the peripherals to have a way of confirming that their data has been received by a central node. As alluded to previously, a central node can indicate to a peripheral node that it has received the advertised data. This is done by sending back a "scan request" ping, which is usually

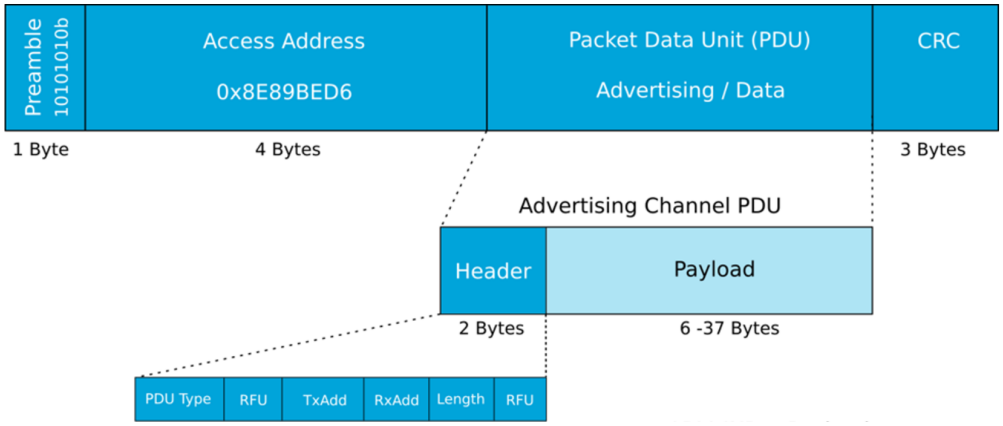

Fig. 8 BLE 4.0 spec for advertising packet [35]

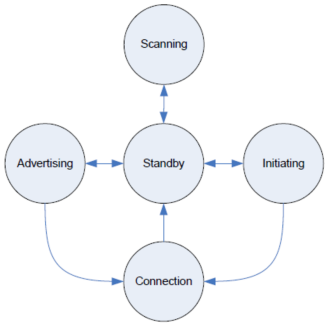

Fig. 9 BLE transition between power states [37]

used to request supplementary information about any previously advertised data [35]. Our peripheral nodes need not respond to this scan request with a scan response (as would usually be the case), but can instead simply log a bit flip to indicate the central node's confirmation of data receipt. Notably, this confirmation of data transfer procedure is much simpler if nodes are fully connected, but we are interested in avoiding that state when possible, in the interest of power conservation. We will implement a procedure for peripherals to become centrals as needed, to take over the data aggregating duties, should they find that their data has not been read for longer than five minutes. This allows us to dynamically update the topology and replace the role of any central node that may have failed.

For additional redundancy considerations, we will deploy the first in-space prototype tests with at least two downlink-capable nodes, should the primary downlink node fail.

IV. Preliminary Results and Deployment Approach

A. Zero Gravity Test Hypotheses

While we position this paper primarily as a concept design review, we have completed initial tests on the proof-of-concept hardware prototype shown in Fig. 2b and will share our preliminary results. Our goal in testing the table-top prototype is to explore the impact of four parameters on the time-scale and completion rate of a self-assembling system. We intend to extrapolate learnings from this hypothesis testing to larger scale deployments in the future.

Circulation: Component parts require sufficient opportunity for the proper joints to find each other and bond. Circulation of the tiles aids in exposing joints for bonding. How much circulation is required for tiles to passively self-assemble, given initial release conditions and the strength of remote attraction between tiles?

Containment: Component parts must be kept proximate for the jointing mechanism to draw tiles together (in our case, driven by magnetic forces). Without an onboard propulsion system, there is no way to direct a tile back to the main assembly group if uncontained. What is the optimum volume of containment, given a target assembly size?

Seeding: Much as a crystal "seed" induces structure nucleation, a properly tuned primitive (a few pre-assembled tiles that seed the correct geometry) may guide the subsequent assembly more efficiently. What is the ideal seed geometry, and do tiles assembly more or less efficiently when a seed primitive is introduced?

Kinetic Disturbance: If, in the process of assembling, certain non-ideal joints form, the self-assembling system should be able to course-correct. One approach is to introduce a kinetic disturbance that perturbs the system and knocks weak, incorrectly bonded joints apart. What magnitude of kinetic disturbance is required to return the system to a properly-assembling state, and can the need for this intervention be predicted?

In Fig. 10, we examine how our iterative testing progression (from a recently completed parabolic flight, to prospective sub-orbital launch, to prospective internal-ISS deployment test) addresses these parameters, given the unique affordances of each deployment environment. While these four parameters are not the sole factors to consider in a self-assembling deployment, we have selected them for their experimental practicality and their fundamental roles in describing a system (system bounds: containment; initial conditions: seeding; initial input energy: circulation; exogenous additional energy to guide the outcome: kinetic disturbance).

	Tests containment?	Tests seeding?	Tests circulation?	Tests kinetic disturbance?
Parabolic Flight Deployment period (15-30 seconds, repeated)	YES	YES	NO	NO
Sub-orbital Flight (3 minutes)	YES	YES	YES	NO
ISS deployment (days to weeks)	YES	YES	YES	YES

Fig. 10 Summary of testing parameters by zero gravity deployment opportunity

Our parabolic flight experimental setup (further details below) provided containment and allowed for seed experiments, but did not include auxiliary fans or other means of circulation. Kinetic disturbance was also not employed, as we desired to observe independent assembly dynamics and later motivate kinetic disturbance if needed. Our upcoming sub-orbital flight will still feature containment and seeding, and will add a circulation mechanism. Finally, an ISS deployment would support all four parameters, as time would allow for system diagnosis, observance of non-ideal jointing and subsequent kinetic disturbance intervention.

B. Parabolic Flight Results

For our November 2017 parabolic flight, we deployed two sets of 32 tiles each. Each set was identical and designed to assemble into a 13cm diameter C60 buckyball structure. The first set was placed in an 18" x 18" x 18" container; the second set was placed in a 14" x 14" x 14" container. We did not deploy the sensor nodes as part of this test–our results discussion centers on camera analysis. As our first zero gravity deployment, this parabolic flight was intended to test:

Baseline performance: do the tiles come together as anticipated and self-assemble via the magnetic joints?

Containment volume: holding all other variables the same, how does containment volume affect the dynamics of assembly?

Figure 11 shows our initial setup, with the tiles arranged on the floor of the two containment boxes. Tiles were arranged in a pre-set pattern in each box prior to the first parabola, and allowed to float free during the repeated periods of microgravity. Though the bottom surface areas of the two boxes are different, an attempt was made to be as consistent as possible in the initial tile placement for the two boxes. During breaks, tiles were re-arranged in preparation for the subsequent string of parabolas. Three regimes were tested: a) all tiles separate, b) seeding method where tiles were pre-assembled into groups of 3-5, and c) hole-filling test where the majority of tiles are pre-assembled and we test the ability of the remaining tiles to fill the holes.

With this parabolic flight test, we were able to validate the basic mechanism of self-assembly and confirm that the tiles are drawn together over a separation distance of several centimeters, over the course of a parabola's 10-15 seconds. We noted successful, independent assembly of subsets of the buckyball geometry, though not the full structure. We observed that the full set of parts gathered together (in various states of expected and unexpected geometries) over a shorter time-scale in the smaller volume box than in the larger volume box, due in part to the increased prevalence of tile-tile interaction. In addition to the hypothesized assembly behavior (constrained to matching magnet joints), we also observed clumping (see Fig. 12), where weak magnetic forces on the top and bottom surfaces of tiles captured neighbor tiles. This was due to the neodymium magnets' extra bonding faces exerting attractive forces through the plastic shell, above and below the recessed holes (rather than solely acting through and bonding via the exposed faces). Fortunately, this presents a clear mitigation strategy: tile designs with greater thickness of plastic above and below the recessed magnet holes (i.e. overall thicker tiles) to more effectively block undesired surface interactions.

Fig. 11 Initial tile layout for parabolic flight test.

Fig. 12 An example of unintentional magnetic interaction between non-bonding faces of the tiles. The remaining assembly (partial buckyball) was manually assembled to test hole-filling in this particular parabola scenario.

V. Summary

At 13cm in diameter, this prototype offers a meaningful, small-scale test of each general element of an adaptive, self-assembling system as identified in the introduction: base unit, jointing method, assembly protocol and holistic function. With fixed hexagon and pentagon tiles, tuned to the proper dihedral angle and embedded with magnets, we have created a base unit that is simple, easily replicated and assembles with neighbors when brought into close proximity. The magnet joint polarity design need only define two unique joints, allowing us greater flexibility in the jointing method and improving the probabilities for predictable assembly in a stochastic system. The assembly protocol–passive, stochastic assembly in zero gravity–was recently validated on our November 2017 parabolic flight. Although clumping behavior precluded a proper, full assembly, we have a clear engineering solution going forward and a spiral development plan that will provide additional opportunities for prototype refinement and deployment. Finally, the sensor nodes and communication architecture will provide critical assembly-process monitoring and contribute to both data-gathering and information-exchange as holistic functions for the structure. This allows us to test a fully networked, sensor-augmented proof of concept prototype for the future of in-orbit habitation structures.

Future work for the self-assembly mechanism will include upgrading the passive, neodymium magnets to electromagnets and completing a kinematics model (with magnetostatics layer) to simulate the stochastic dynamics. We propose extensive modeling to understand and characterize the tiles' stochastic assembly dynamics over a range of orbiting environments, for various target structure sizes, for certain magnet strengths, and for various assembly-containment volumes. We may also explore a hybrid propulsion and magnets model, where coarse propulsion is used to achieve a certain general "quadrant" location and electromagnets are subsequently turned on to aid in closer-proximity docking. In addition to the assembly kinematics model, we are interested in energy-of-the-formation vs time, and considering threshold scenarios where the energy of the colliding system passes from effective to destructive (as tile mass increases in subsequent deployment contexts). We will continue to iterate on the sensor node and communication architecture and will prepare a new version of the PCBs that are space-qualified and uplink/downlink enabled.

With this project, we hope to explore a new era in the trajectory of space architecture. We look ahead, to the technology needs of the next 15-30 years, to support the first significant waves of humans traveling in zero gravity (from space tourists to asteroid miners). We will need flexible means of accommodating humans in orbit, as staging locations for further exploration and the pursuit of interplanetary life. The ease with which we can deploy, reconfigure and adapt our habitats will directly impact the success of space missions—from lowering costs, to improving safety via fewer astronaut EVAs, to enabling agile and rapid infrastructure response for operation needs. We look forward to developing a suite of technologies that brings innovation to space structures development in the near term, while also shaping a bold vision for human life and work in orbit–wherever our orbits may be.

Acknowledgments

The authors would like to thank Brian Mayton, of the Responsive Environments group at the MIT Media Lab, for his aid in re-purposing the tidmarsh solar charging circuit components. We would also like to thank Professor Kerri Cahoy, instructor for the MIT AeroAstro 16.343 course in which the sensor application approach for this project was designed and refined. This work is supported by the MIT Media Lab consortium and the MIT Media Lab Space Exploration Initiative.

References

[1] Reusability: The Key to Making Human Life Multi-Planetary. SpaceX. 10 Jun 2015. [Online] http://www.spacex.com/news/2013/03/31/reusability-key-making-human-life-multi-planetary

[2] Aguirre,E. Prof Awarded NASA Grant to Develop Building Blocks for Use in Space Missions. UMASS Lowell. 5 Jan 2015. [Online] https://www.uml.edu/Research/news/Hansen-NASA-grant.aspx.

[3] Kroto, Harold W., James R. Heath, Sean C. O'Brien, Robert F. Curl, and Richard E. Smalley. "C60: Buckminsterfullerene." Nature 318, no. 6042 (1985): 162-163.

[4] Langford, Will, Amanda Ghassaei, and Neil Gershenfeld. "Automated Assembly of Electronic Digital Materials." In ASME 2016 11th International Manufacturing Science and Engineering Conference, pp. V002T01A013-V002T01A013. American Society of Mechanical Engineers, 2016.

[5] Gershenfeld, Neil, Matthew Carney, Benjamin Jenett, Sam Calisch, and Spencer Wilson. "Macrofabrication with Digital Materials: Robotic Assembly." *Architectural Design* 85, no. 5 (2015): 122-127.

[6] Cheung, Kenneth C and Neil Gershenfeld. Reversibly assembled cellular composite materials. *Science* 341, no. 6151 (2013): 1219-1221.

[7] Chiral Self-assembly. MIT Self-assembly Lab. [Online] Accessed 25 May 2017. http://www.selfassemblylab.net/ChiralSelfAssembly.php

[8] Self-folding Surfaces. MIT Self-assembly Lab. [Online] Accessed 25 May 2017. http://www.selfassemblylab.net/SelfFoldingSurfaces.php

[9] Biased Chains. MIT Self-assembly Lab. [Online] Accessed 25 May 2017. http://www.selfassemblylab.net/BiasedChains.php

[10] Mayton, B., Dublon, G., Russell, S., Lynch. E.F., Haddad, D.D., Ramasubramanian, V., Duhart, C., Davenport, G., and Paradiso, J.A., "The Networked Sensory Landscape: Capturing and Experiencing Ecological Change Across Scales," to appear in Presence, 2018. See tidmarsh.media.mit.edu for more information.

[11] Rubenstein, Michael, Alejandro Cornejo, and Radhika Nagpal. "Programmable self-assembly in a thousand-robot swarm." *Science* 345, no. 6198 (2014): 795-799.

[12] Bobrow, Jonathan. "AutomaTiles: tangible cellular automata for playful engagement with systems thinking." PhD diss., Massachusetts Institute of Technology, 2016.

[13] Paradiso, J.A., Lifton. J., and Broxton, M., "Sensate Media - Multimodal Electronic Skins as Dense Sensor Networks," BT Technology Journal, 22(4), October 2004, pp. 32-44.

[14] Bigelow Expandable Activities Module (BEAM). Bigelow Aerospace and NASA. [Online] Accessed 9 September 2017. https://www.nasa.gov/content/bigelow-expandable-activity-module

[15] Seager, Sara, Margaret Turnbull, William Sparks, Mark Thomson, Stuart B. Shaklan, Aki Roberge, Marc Kuchner et al. "The Exo-S probe class starshade mission." SPIE, 2015.

[16] "Growth-adapted Tensegrity Structures–a new calculus for the space economy." NASA NIAC Phase I and II Project. July 2013. [Online] Accessed 23 November 2017. https://www.nasa.gov/content/growth-adapted-tensegrity-structures-a-new-calculus-for-the-space-economy

[17] Liu, Ke, Jiangtao Wu, Glaucio H. Paulino, and H. Jerry Qi. "Programmable Deployment of Tensegrity Structures by Stimulus-Responsive Polymers." Scientific reports 7, no. 1 (2017): 3511.

[18] Leveraging Space for Industry: beyond exploration. Made in Space. [Online] Accessed 25 May 2017. madeinspace.us/solutions-overview/self

[19] Gumennik, Alexander, Etgar C. Levy, Benjamin Grena, Chong Hou, Michael Rein, Ayman F. Abouraddy, John D. Joannopoulos, and Yoel Fink. "Confined in-fiber solidification and structural control of silicon and silicon-germanium microparticles." Proceedings of the National Academy of Sciences (2017): 201707778.

[20] Zheng, Wen, Qingmei Cheng, Dunwei Wang, and Carl V. Thompson. "High-performance solid-state on-chip supercapacitors based on Si nanowires coated with ruthenium oxide via atomic layer deposition." Journal of Power Sources 341 (2017): 1-10.

[21] ATMEL 8-BIT MICROCONTROLLER WITH 4/8/16/32KBYTES (328p). Atmel. [Online] Accessed 25 May 2017. http://www.atmel.com/images/atmel-8271-8-bit-avr-microcontroller-atmega48a-48pa-88a-88pa-168a-168pa-328-328p_datasheet_summary.pdf

[22] Ultra-compact high-performance eCompass module: 3D accelerometer and 3D magnetometer (lsm303dlhc). ST Microelectronics. [Online] Accessed 25 May 2017. http://www.st.com/content/ccc/resource/technical/document/datasheet/56/ec/ac/de/28/21/4d/48/DM00027543.pdf/files/DM00027543.pdf/jcr:content/translations/en.DM00027543.pdf

[23] MEMS motion sensor: ultra-stable three-axis digital output gyroscope (l3g4200dtr). ST Microelectronics. [Online] Accessed 25 May 2017. http://www.st.com/content/ccc/resource/technical/document/datasheet/04/46/d6/00/be/d9/46/ae/CD00265057.pdf/files/CD00265057.pdf/jcr:content/translations/en.CD00265057.pdf

[24] Bluetooth V4.0 HM-11 BLE Module. Seeed. [Online] Accessed 25 May 2017. http://wiki.seeed.cc/Bluetooth_V4.0_HM_11_BLE_Module/

[25] bq25570 Nano Power Boost Charger and Buck Converter for Energy Harvester Powered Applications. Texas Instruments. [Online] Accessed 25 May 2017. http://www.ti.com/lit/ds/symlink/bq25570.pdf

[26] Li-Polymer Battery Technology Specification. Shenzen PKCELL Battery Co., LTD. [Online] Accessed 25 May 2017. https://cdn-shop.adafruit.com/product-files/1570/1570datasheet.pdf

[27] IXOLAR High Efficiency SolarBIT. IXYS. [Online] Accessed 25 May 2017. http://ixapps.ixys.com/DataSheet/KXOB22-01X8F_Nov16.pdf

[28] Technical Documents: Ultra Low Power Harvester Power Management IC with Boost Charger, and Nanopower Buck Converter. Texas Instruments. [Online] Accessed 25 May 2017. http://www.ti.com/product/BQ25570/technicaldocuments

[29] Proximity sensor, gesture and ambient light sensing (ALS) module. ST Microelectronics. [Online] Accessed 25 May 2017. http://www.st.com/en/imaging-and-photonics-solutions/vl6180x.html

[30] World smallest Time-of-Flight (ToF) ranging sensor. ST Microelectronics. [Online] Accessed 25 May 2017. http://www.st.com/en/imaging-and-photonics-solutions/vl53l0x.html

[31] Adafruit VL6180X Time of Flight Distance Ranging Sensor (VL6180). Adafruit. [Online] Accessed 25 May 2017. https://www.adafruit.com/product/3316

[32] SparkFun ToF Range Finder Sensor - VL6180. Sparkfun. [Online] Accessed 25 May 2017. https://www.sparkfun.com/products/12785

[33] Adopted Specifications. Bluetooth Special Interest Group. [Online] Accessed 25 May 2017. https://www.bluetooth.com/specifications/adopted-specifications

[34] Bluetooth Basics. Sparkfun. [Online] Accessed 25 May 2017. https://learn.sparkfun.com/tutorials/bluetooth-basics

[35] A BLE Advertising Primer. Argenox. [Online] Accessed 25 May 2017. http://www.argenox.com/a-ble-advertising-primer/

[36] ibeacon. Apple Developer Kit. [Online] Accessed 25 May 2017. https://developer.apple.com/ibeacon/

[37] Technical Considerations. Bluetooth Special Interest Group. [Online] Accessed 25 May 2017. https://www.bluetooth.com/specifications/bluetooth-core-specification/technical-considerations